NeuroImage **15,** 697–707 (2002)
doi:10.1006/nimg.2001.1021, available online at http://www.idealibrary.com on IDEAL®

Improved Parametric Image Generation Using Spatial-Temporal Analysis of Dynamic PET Studies

Yun Zhou, Sung-Cheng Huang,* Marvin Bergsneider,† and Dean F. Wong

*The Russell H. Morgan Department of Radiology and Radiological Science, Johns Hopkins Medical Institutions, Baltimore, Maryland 21287; and *Department of Molecular and Medical Pharmacology, †Division of Neurosurgery and Brain Injury Research Center, School of Medicine, University of California at Los Angeles, California 90095*

Received July 23, 2001; published online January 22, 2002

The value of parametric images that represent both spatial distribution and quantification of the physiological parameters of tracer kinetics has long been recognized. However, the inherent high noise level of pixel kinetics of dynamic PET makes it unsuitable to generate parametric images of the microparameters of tracer kinetic model by conventional weighted nonlinear least squares (WNLS) fitting. Based on the concept that both spatial and temporal information should be integrated to improve parametric image quality, a nonlinear ridge regression with spatial constraint (NLRRSC) parametric imaging algorithm was proposed in this study. For NLRRSC, a term that penalizes local spatial variation of parameters was added to the cost function of WNLS fitting. The initial estimates and spatial constraint were estimated by component representation model (CRM) with cluster analysis. A hierarchical cluster with average linkage method was used to extract components. The ridge parameter was determined by linear ridge regression theory at each iteration, and a modified Gauss–Newton algorithm was used for minimizing the cost function. Results from a computer simulation showed that the percent mean square error of estimates obtained by NLRRSC can be decreased by 60–80% compared to that of WNLS. The parametric images estimated by NLRRSC are significantly better than the ones generated by WNLS. A highly correlated linear relationship was found between the ROI values calculated from the microparametric images generated by NLRRSC and estimates from ROI kinetic fitting. NLRRSC provided a reliable estimate of glucose metabolite uptake rate with a comparable image quality compared to Patlak analysis. In conclusion, NLRRSC is a reliable and robust parametric imaging algorithm for dynamic PET studies.

INTRODUCTION

The analysis of dynamic positron emission tomography (PET) studies utilizing a compartmental tracer kinetic model is an established technique for measuring biological function *in vivo*. The quantification of individual model parameters (termed microparameters) can improve the understanding of the relative contribution of delivery, transport, and biochemical transformation of molecules within the body. We have been interested particularly in determining the transport and phosphorylation rates of [F-18]fluorodeoxyglucose (FDG) in the brain in order to better understand the marked changes in the cerebral glucose metabolism acutely following traumatic brain injury (Bergsneider *et al.*, 1997). These microparameters typically are estimated by fitting the model to the tissue time activity curve (TAC) obtained from the dynamic PET study. The ability to derive the "true" representative fitted curve is dependent upon the quality of the TAC. In many pathological states, including traumatic brain injury, reduced or altered tracer uptake during PET studies can result in highly noisy TACs assessed for individual pixels, and therefore, lead to inaccurate or invalid estimates of the microparameters due to poor fitting or nonconvergence.

A simple method used to circumvent the problem of noise in TACs in estimating microparameters is to draw a large region-of-interest (ROI) and apply it to the dynamic image set. The averaging of pixel values enclosed within each ROI reduces the noise level in the TAC thereby improving the accuracy and efficiency of the curve-fitting regression procedure. Using this so-called "ROI method," either general linear regression or nonlinear regression can be easily and reliably applied to estimate model parameters defined in the kinetic model. One drawback of this approach is that the ROIs must be drawn in advance without an indication of the regional variability of the microparameters in question. As a result, identifying regional patterns using the ROI method may be a labor intensive trial-and-error process. In addition, a high heterogeneity of kinetics within an ROI may introduce significant errors into the estimates. (Herscovitch and Raichle, 1983;

1053-8119/02 $35.00

Herholz and Patlak, 1987; Blomqvist *et al.*, 1995; Wu *et al.*, 1995; Zhou *et al.*, 1997).

An alternative to the above ROI method is the generation of a parametric image representing a given microparameter based on modeling the tracer kinetics for each individual pixel in the image volume. Parametric images that represent both spatial distribution and quantitation of the physiological parameters are highly desirable for data presentation and analysis. The model independent graphical analysis (Patlak *et al.*, 1983; Patlak and Blasber, 1985; Logan *et al.*, 1990, 1996; Choi *et al.*, 1991) and spectral analysis (Cunningham and Jones, 1993) were most often used to generate macroparametric images, a function of micro parameters of tracer kinetic model such as uptake rate constant ($K_i = K_1k_3/(k_2 + k_3)$) in FDG or irreversible tracer studies and distribution volumes ($DV = (K_1/k_2)(1 + k_3/k_4)$) in ligand–receptor studies. With approximation and model simplification, linear parametric imaging algorithms have been developed for generating microparametric images (Blomqvist 1984, 1990; Carson *et al.*, 1986; Frey *et al.*, 1991; Koeppe *et al.*, 1991; Feng *et al.*, 1996; Gunn *et al.*, 1997; Chen *et al.*, 1998; Zhou *et al.*, 2001a, 2001c). Traditionally, most parametric mapping theories and algorithms for dynamic PET studies have been based on linear and nonlinear regression. Linear parametric imaging algorithms offer the greatest simplicity and computational efficiency. Nonlinear regression, such as weighted nonlinear least squares (WNLS) fitting, is a more general method compared to its linear counterpart. Unfortunately, due to the high noise level of pixel kinetics, the parametric images generated by conventional WNLS method are usually of poor image quality, i.e., either too noise or too much resolution loss if spatial smoothing is applied.

To improve the quality of parametric images generated by WNLS, several strategies were developed to reduce the random fluctuations in the TAC. One method involves spatial filtering applied on dynamic images by local likelihood-type procedures (Herholz, 1987). Although this is effective in lowering the noise component, the technique requires excessive computational time for routine use. This type of approach can be improved by a so called "mixture analysis" (O'Sullivan 1994), in which the component representation model (CRM) used is based on the assumption that each pixel can be expressed linearly in terms of components both in the kinetic space and the parameters space. The parametric images generated by this algorithm are sensitive to the accuracy of the estimated components and the algorithms for extracting appropriate components can become complex and computationally costly.

As an alternative to applying spatial smoothing to the dynamic images, we developed a constraint method to reduce variation in the parameter space during nonlinear regression. Intermediate estimates obtained at each iteration during nonlinear regression were spatially smoothed (Huang and Zhou, 1998). This spatial constraint parametric imaging algorithm was modified further by the addition of nonlinear simple ridge regression with spatial constraint (NLRRSC) (Zhou *et al.*, 2001b). NLRRSC theory takes the strategy of minimizing the cost function by including a local spatial constraint (penalty) in the parameter space. In that algorithm, the same initial estimates and constraints were estimated by model fitting to the whole brain tissue average kinetics. The spatial constraints were updated at each iteration, and a Gauss–Newton with half step algorithm was used.

The purpose of the current study is to decrease the bias of NLRRSC estimates and to improve convergence by (a) providing a more accurate initial estimate, (b) fixing the spatial constraint, and (c) using more efficient step search algorithm during nonlinear regression. Hierarchical cluster analysis with average linkage method is used to extract components for the CRM analysis. The initial estimates are then adjusted by nonlinear regression with fixed spatial constraint. The details of the NLRRSC algorithm are described in the following sections.

MATERIALS AND METHODS

Theory and Algorithm

As described in the Introduction section, there are three steps to implement NLRRSC: (1) Hierarchical cluster analysis with average linkage method is applied to the dynamic image data. Components in the kinetic space and the parameter space are then extracted by fitting the tracer kinetic model to the kinetics of each cluster. (2) Images of the initial estimates and constraints are then obtained by CRM analysis. (3) Initial estimates are adjusted by minimizing the cost function using nonlinear regression with spatial constraint.

To extract components in the kinetic space, hierarchical cluster analysis with average linkage method (Anderberg, 1973) is used to partition the dynamic PET image data sets into a preselected number of clusters. The clusters selected for further analysis must include an adequate number (depending upon noise level) of pixels during the clustering process so that the mean kinetics of each cluster has a high signal-to-noise ratio for WNLS model fitting. The components in the parameter space and the kinetic space are then obtained by fitting the model to the kinetics of the cluster means. Let us assume that N clusters are obtained for a given data set of dynamic PET images, and its corresponding cluster means are $Z_1, Z_2, \ldots, Z_N$, respectively. Weighted nonlinear regression using the Marquardt algorithm (Marquart, 1963), a standard WNLS fitting algorithm, is used to fit model to the cluster means Z_i.

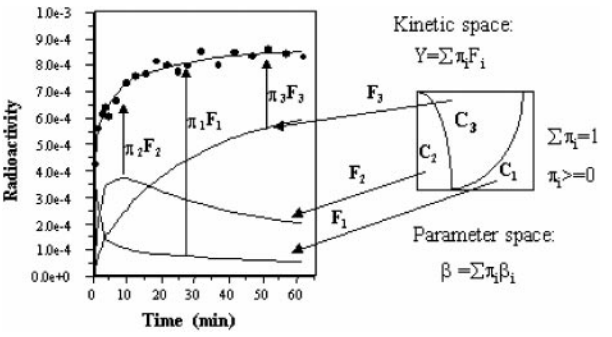

FIG. 1. Linear components representation model. Given components $\{F_i\}$ in the kinetic space and the corresponding components $\{\beta_i\}$ in the parameter space, the linear relationship between the pixel and components in the kinetic space is also true in the parameter space. The contributions from each component (π_i) could be estimated by non-negative linear least square fitting in the kinetic space.

The ith component in the parameter space and the kinetic space is determined by minimizing the cost function below:

$$Q_i = (Z_i - F(\beta))' W (Z_i - F(\beta)), \tag{1}$$

where $'$ is mathematical transpose operation, $1 \le i \le N$. We let $F_i = F(\beta^{(i)})$, where $\beta^{(i)}$ is estimated by minimizing the cost function Q_i. Then the fitted $\{F_i\}$ and estimated $\{\beta^{(i)}\}$ are the components in the kinetic space and in the parameter space, respectively.

Based on the extracted components (F_i, $\beta^{(i)}$, $1 \le i \le$ N), the CRM is used to provide the initial estimates and parameter constraints. As illustrated in Fig. 1, CRM assumes that kinetics for each pixel can be represented by a linear combination of the extracted components, i.e.:

$$Y_j = \sum_{i=1}^{N} \pi_{ij} F_i, \tag{2}$$

where Y_j is the measurement of pixel j, $\pi_{ij} \ge 0$ and $\Sigma_i \pi_{ij} = 1$. By applying constraint to the linear regression, the weight π_{ij} is estimated. So the model parameter at jth pixel is roughly estimated by:

$$\beta_j = \sum_{i=1}^{N} \pi_{ij} \beta^{(i)}. \tag{3}$$

We let $S\beta_j$ be the spatially smoothed β_j. The initial estimates β_0 and the constraint β_s for NLRRSC are both set to equal to $S\beta_j$ for pixel j:

$$\beta_{0j} = S\beta_j \tag{4}$$

$$\beta_{sj} = S\beta_j \tag{5}$$

As described below, β_0 is used as the initial parametric image for nonlinear regression, and the spatial constraint image β_s is fixed in the nonlinear regression of NLRRSC.

In the last step of NLRRSC, the initial estimates are adjusted by minimizing the following total sum of squares (TSS) which includes weighted residual sum of squares in the kinetic space and a term penalizing the local spatial variation in the parameter space, i.e.,

$$\mathrm{TSS} = (F(\beta) - Y)' W (F(\beta) - Y) + h(\beta - \beta_s)'(\beta - \beta_s), \tag{6}$$

where Y ($n \times 1$) is the vector of n temporal measurements of tissue radioactivity, β ($m \times 1$) is the parameter vector to be estimated, $F(\beta)$ ($n \times 1$) is the predicted value from the tracer kinetic model, and W is the diagonal matrix whose positive diagonal elements w_{ii} usually reflect the accuracy of measurement at the ith time point. For the following simulation and human studies, the diagonal elements w_{ii} = (duration of ith frame of PET dynamic scanning) was used. The term $h(\beta - \beta_s)'(\beta - \beta_s)$ reflects the penalty on spatial variation in the parameter space, and h is usually called the ridge parameter or penalty coefficient. TSS is minimized by the conventional nonlinear least squares optimization procedure. Based on the performance and computation efficiency, a modified Gauss–Newton algorithm for searching step size was used in the NLRRSC for nonlinear regression (Hartley, 1961), and it was implemented as shown in the following procedure. At each iteration of the nonlinear regression, starting with β_I estimated in the previous iteration, and using the first order approximation of $F(\beta_I + \Delta\beta)$,

$$F(\beta_I + \Delta\beta) = F(\beta_I) + (dF/d\beta)\Delta\beta, \tag{7}$$

where $dF/d\beta$ ($n \times m$) is the gradient of F at β_I on the parameter space, the step $\Delta\beta$ is determined by minimizing the cost function below in the current iteration.

$$\begin{aligned} Q(\Delta\beta) = {} & (F(\beta_I) + (dF/d\beta)\Delta\beta - Y)' W (F(\beta_I) \\ & + (dF/d\beta)\Delta\beta - Y) \\ & + h(\beta_I + \Delta\beta - \beta_s)'(\beta_I + \Delta\beta - \beta_s). \end{aligned} \tag{8}$$

To determine $\Delta\beta$, the theory of linear simple ridge regression with spatial constraint is applied for optimization of the ridge parameter h (Zhou *et al.*, 2001a). That is, based on Eq. (8), an intermediate h_a is obtained using Eq. (9) and (10) below.

$$\Delta\beta_a = ((dF/d\beta)' W (dF/d\beta))^{-1} ((dF/d\beta)' W (Y - F(\beta_I)) \tag{9}$$

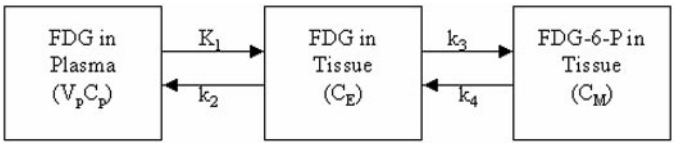

FIG. 2. Compartment model used to simulate tissue FDG kinetics. V_pC_p is the FDG plasma concentration in vascular space; C_E is the free FDG concentration in tissue; C_M is phosphorylated FDG concentration in tissue. V_p is the fractional plasma volume in vascular space, and K_1–k_4 are the rate constants.

$$h_a = m((F(\beta_I) + (dF/d\beta)\Delta\beta_a - Y)' W(F(\beta_I) + (dF/d\beta)\Delta\beta_I - Y)/(n - m))/ ((\beta_I + \Delta\beta_a - \beta_s)'(\beta_I + \Delta\beta_a - \beta_s)). \quad (10)$$

Afterward, h_a is spatially smoothed to give the ridge parameter h. A modified Gauss–Newton algorithm is then used to calculated the step $\Delta\beta$ through its magnitude ρ and direction θ (i.e., $\beta_{I+1} = \beta_I + \Delta\beta = \beta_I + \rho\theta$), for the next iteration (Hartely, 1961), as determined by Eqs. (11) and (12) below:

$$\theta = ((dF/d\beta)' W(dF/d\beta) + hI_m)^{-1} \times ((dF/d\beta)' W(Y - F(\beta_I) + h(\beta_s - \beta_I)) \quad (11)$$

$$\rho = \frac{0.75Q(0) - Q(0.5\theta) + 0.25Q(\theta)}{Q(0) - 2Q(0.5\theta) + Q(\theta)}. \quad (12)$$

A relative convergence criterion is used to stop the iterations. That is, the iterations are considered to have converged if the total pixel-wise cost function values (summing over all pixels on the image) changes less then 0.1%. That is, the iteration terminates, when

$$\left| \frac{\sum Q(\Delta\beta) - \sum Q(0)}{\sum Q(0)} \right| < 1e-3.$$

Computer Simulation

A 3-compartment 5-parameter model (Phelps *et al.*, 1979; Huang *et al.*, 1980; Hawkins *et al.*, 1986) is used to simulate tissue FDG kinetics. As is illustrated in Fig. 2, the tracer concentrations in the three compartments are C_P, C_E, and C_M, and the rates of changes in concentration are described by Eqs. (13) and (14):

$$\frac{dC_E(t)}{dt} = K_1C_p(t) - (k_2 + k_3)C_E(t) + k_4C_M(t) \quad (13)$$

$$\frac{dC_M(t)}{dt} = k_3C_E(t) - k_4C_M(t). \quad (14)$$

Where $Cp(t)$ is the FDG time activity curve in plasma (the input function), K_1 (ml/min/g) is the forward transport rate constant of FDG from plasma across the blood brain barrier (BBB) to brain tissue, k_2 (1/min) is the reversed transport across the BBB, k_3 (1/min) is the phosphorylation rate constant, and k_4 (1/min) is the de-phosphorylation rate constant. The measured radioactivity by PET scanner (C_T) is the total amount of tracer in tissue and the vascular space:

$$C_T = C_E + C_M + V_pC_p, \quad (15)$$

where V_p (ml/g) is the fractional plasma volume in tissue. From Eqs. (13), (14), and (15), C_T can be expressed in terms of the input function C_p as:

$$C_T = \frac{K_1}{\alpha_2 - \alpha_1}[(k_3 + k_4 - \alpha_1)e^{-\alpha_1 t} + (\alpha_2 - k_3 - k_4)e^{-\alpha_2 t}] \otimes C_p(t) + V_pC_p(t). \quad (16)$$

Where $\otimes$ denotes the convolution operation, and

$$\alpha_1 = [k_2 + k_3 + k_4 - \sqrt{(k_2 + k_3 + k_4)^2 - 4k_2k_4}]/2 \quad (17)$$

$$\alpha_2 = [k_2 + k_3 + k_4 + \sqrt{(k_2 + k_3 + k_4)^2 - 4k_2k_4}]/2. \quad (18)$$

Equation (16) was used to simulate brain tissue kinetics. The parameter vector β ($[K_1\ k_2\ k_3\ k_4\ V_p]'$) of value of [0.102 0.13 0.062 0.004 0.05]) for gray matter and [0.04 0.08 0.029 0.004 0.03]) for white matter was selected from the literature (Phelps *et al.*, 1979; Huang *et al.*, 1980). A FDG plasma TAC from a human PET study was used as the input function. Spatial configuration of gray and white matter on the simulated images followed the Hoffman's phantom (Hoffman *et al.*, 1983). The scanning sequence (4×0.5, 4×4, 10×5 min, total 60 min, over 18 frames) was identical to the human FDG dynamic PET study (see below). Pseudo random noise (normally distributed with its variance proportional to its mean) was added to each simulated data point in the sinogram. Three different noise levels (high: 6×10^6, middle: 10×10^6, and low: 30×10^6 total counts per plane over 60 min) were simulated in the sinogram. For simplification, the processes of attenuation, random, and scatter were not simulated. A Hanning filter with a cutoff at Nyquist frequency was used for image reconstruction (image matrix size 128×128, pixel size 0.125 cm). Twenty realizations for each noise level were obtained for evaluating the statistical properties of the estimates or the parametric images. A 2-D spatial linear smoothing filter (in plane, window size 5×5, equal weighting for all pixels of filter) was used for spatial smoothing in NLRRSC. Parametric images obtained from dynamic images that are reconstructed

from noise-free sinogram were used as the "true" images for error analysis of the images from noisy simulations.

NLRRSC and WNLS were used to generate parametric images from the simulated FDG images. Parametric images of the FDG uptake rate K_i ($= K_1k_3/(k_2 + k_3)$) were generated from the estimated images of K_1, k_2, and k_3. The value of the parameter k_4 was fixed at its true value (0.004/min used in simulation) during model fitting because the total scanning time of dynamic study was only 60 min. Generally, this is not long enough to provide a reliable estimate of k_4 (Huang *et al.*, 1981, 1998; Heiss *et al.*, 1981; Lammertsma *et al.*, 1987). It has been shown that fixing k_4 decreases the k_4-related error to that due to the discrepancy between the actual and the assumed value of k_4 (Jovkar *et al.*, 1989).

While WNLS estimator is unbiased, NLRRSC estimates could be biased. Thus, a useful criterion for accuracy comparison of the two estimator is the percentage of the root mean square error (RMSE%) (Cochran, 1977; O'Sullivan and Saha, 1999), which is defined in Eq. (19). To evaluate the cost of variance reduction for NLRRSC, the percent bias (Bias%) of estimate was calculated using Eq. (20) for results obtained from computer simulation.

$$\mathrm{RMSE\%} = \frac{1}{p}\sqrt{\frac{\sum_{i=1}^{N}(p_i - p)^2}{N-1}} \tag{19}$$

$$\mathrm{Bias\%} = \frac{1}{p}\sum_{i=1}^{N}\frac{(p_i - p)}{N} \tag{20}$$

In Eqs. (19) and (20), p_i is the parameter estimate, p is the "true" value (from noise free simulation), and N is the number of repeated realizations.

Application to Human FDG Dynamic Study

A FDG-PET study in a normal, healthy young adult was analyzed. The study was approved by UCLA Human Subject Protection committee. FDG (~4 mCi) was injected intravenously as a bolus with dynamic image acquisition using a sequence of 4 × 0.5, 4 × 2, 10 × 5 min for a total 60 min (18 frames). A Siemens/CTI ECAT HR+ scanner in 3-D acquisition mode (septa out) was used. Arterial blood samples were taken during the scan and counted in a gamma well counter to derive the plasma FDG time activity curve as the input function. Three blood samples were obtained at equal intervals over the 60-min study for determination of the averaged plasma glucose concentration. This value was used for the calculation of local cerebral metabolic rate of glucose (LCMRGlc). Dynamic images (128 × 128, pixel size = 0.1446 cm, plane separation 0.2425 cm, 63 planes for each frame) were reconstructed using filtered back projection with a Hanning-0.5 filter. Equation (16) was used to fit tissue kinetics (k_4 was fixed at 0.004/min during fitting).

The WNLS was employed for ROI and cluster kinetic fitting. For comparison, NLRRSC and WNLS were applied to the same data set with the same initial estimates obtained by the CRM with cluster analysis for generating parametric images. The 2-D spatial linear smoothing filter (in plane, window size 5 × 5, equal weighting for all pixels of filter) that was used in the computer simulation was also used in human study. For evaluating the reliability of the NLRRSC method with real data, ROI averages of estimates calculated from parametric images were compared to those obtained by fitting model to ROI kinetics. The ROIs contained at least 20 pixels and were defined on a set of planes that included gray matter, white matter, sinus, and combined regions. The LCMRGlc was calculated with the following equation:

$$\mathrm{LCMRGlc} = (C_{pg}/\mathrm{LC})K_i, \tag{21}$$

where C_{pg} is the glucose concentration in plasma (mg/100 ml) and LC is the lumped constant. Here, a historical value of LC = 0.42 (Phelps *et al.*, 1979; Huang *et al.*, 1980) was used for the entire brain. As a comparison, a parametric image of LCMRGlc was also estimated by the Patlak method, which is currently a common technique for LCMRGlc estimation and is independent of the specific model structure. Pixel-wise comparison of LCMRGlc obtained with NLRRSC and Patlak plot was also examined.

The NLRRSC and WNLS were written in MATLAB (The MathWorks Inc.) code, and implemented on an Ultra 5 SPARC workstation (Sun Microsystems, Inc., Palo Alto, CA).

RESULTS

Computer Simulation

Figure 3 showed the accuracy of the estimates (whole brain average RMSE% of K_1, k_2, k_3, V_p) at the various noise levels. Both NLRRSC and WNLS parametric imaging methods revealed that k_2, k_3, and V_p are more sensitive to noise level than for K_1. The sensitivity (based on the slope of regression line) of k_3 was highest for both WNLS and NLRRSC methods. By comparing the NLRRSC with WNLS estimates, the whole brain average RMSE% of NLRRSC estimates is less than 60–80% of those of WNLS estimates. This improvement in the estimates of K_1, k_2, k_3, and V_p by NLRRSC gives an RMSE% reduction for K_i ($K_1k_3/(k_2 + k_3)$) of 60–80% as compared to the WNLS estimates. Results for gray and white matter values were also found to be similar.

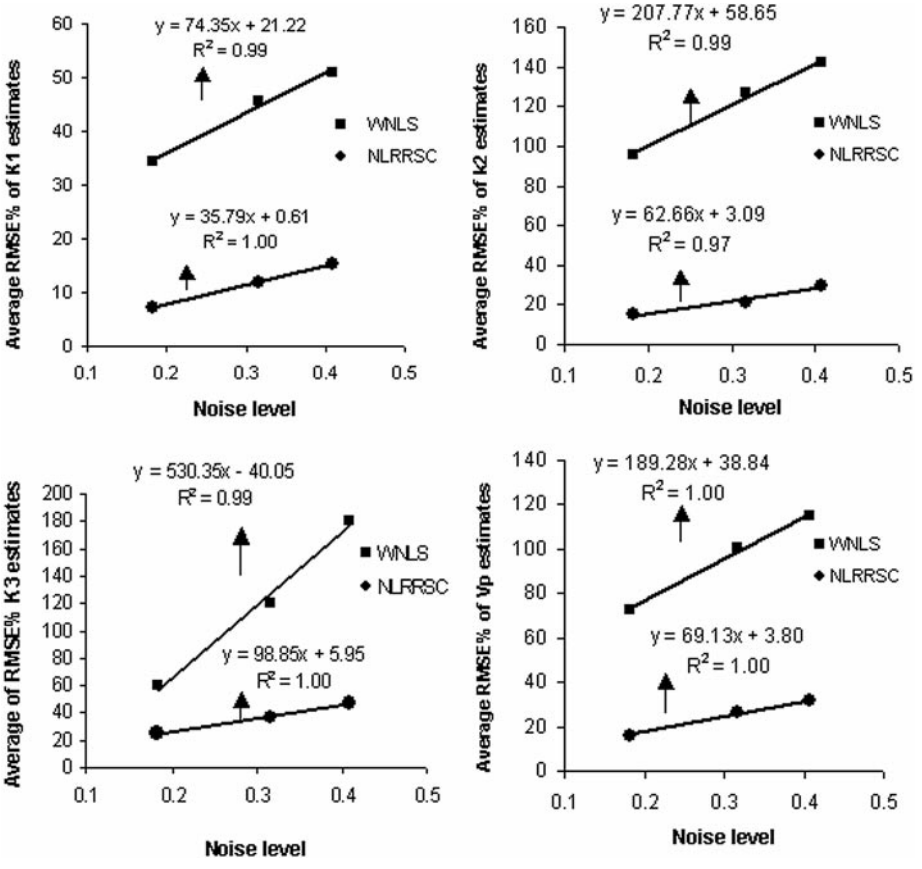

FIG. 3. Whole brain average RMSE% of WNLS and NLRRSC estimates for three noise levels (the scale is proportional to 1/(total counts)$^{1/2}$). The same initial estimates were used in WNLS and NLRRSC. The smoothing filter with 5 × 5 pixel window size was used for NLRRSC.

A representative example of pixel-wise comparison of model fitting is shown in Fig. 4. The single pixel was selected from a gray matter region in one realization of a midnoise level simulation. The parameter vector [K_1, k_2, k_3, V_p] from the "true" parametric images reconstructed from noise free phantom sinogram was [0.101, 0.131, 0.062, 0.050] for that particular pixel. The parameters estimated by the NLRRSC and WNLS methods were [0.101, 0.129, 0.055, 0.050] and [0.196, 0.390, 0.072, 0.003], corresponding to residual sum of squares of 8.49×10^{-7} and 8.31×10^{-7}, respectively. Generally, WNLS gave a lower residual sum of squares than that obtained by NLRRSC, but is more sensitive to the noise level of pixel kinetics. This example revealed that, without constraint, the lower residual sum of squares of WNLS fitting occurs at the cost of higher variation in the parameter space. This also demonstrated that the strategy of minimizing the residual sum of squares with spatial constraint or penalty reduces the variability of the estimates.

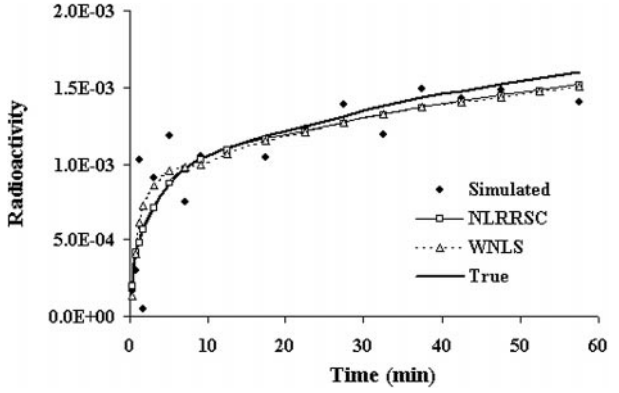

FIG. 4. Evaluation of the model fitting at pixel level for WNLS and NLRRSC. WNLS gave lower residual sum of squares at the cost of the higher deviation from "true" in parameters space. The radioactivity unit on the y axis is proportional to μCi/ml.

The average Bias% of estimates decreased as the noise level became smaller. The Bias% of NLRRSC estimates (K_1, k_2, k_3, V_p, K_i,) in gray matter was less than ±5% at the high noise level. For white matter, the average Bias% of the linear parameter estimates K_1, and V_p, were less than ±10% at the high noise level, while the average Bias% of the nonlinear parameters k_2 and k_3 could be up to 20%. The average Bias% of K_i

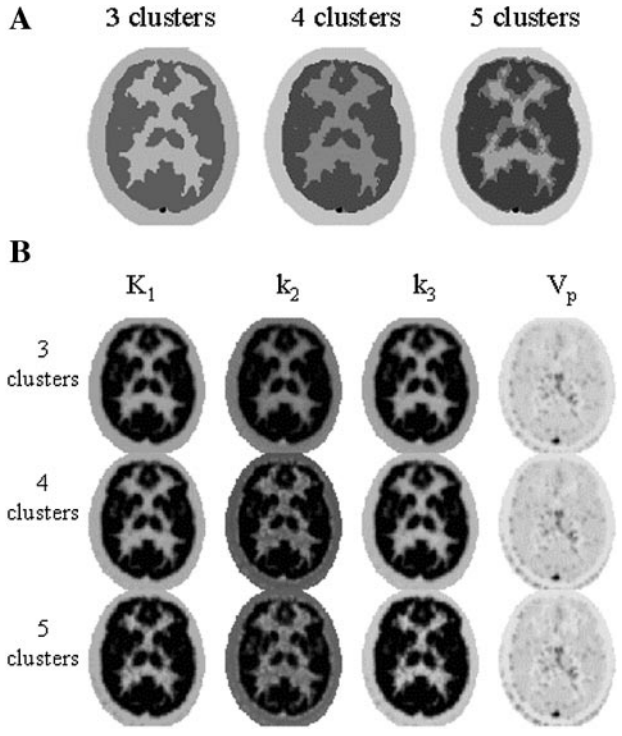

FIG. 5. Results of clustering for one slice level from hierarchical cluster with average method (A) and corresponding initial estimates and spatial constraint to be used in NLRRSC (B).

was less than 5% at all noise levels. The main factor contributing to the bias of NLRRSC estimates was due to the ridge regression (Hoerl and Kennard, 1970a, 1970b; O'Sullivan and Saha, 1999). It should be noted that (1) the bias of NLRRSC estimates is negligible if compared to the variance of the estimates; and (2) in real dynamic PET studies, many other factors in the real world, such as scatter and attenuation process, model simplification of tracer kinetic, may cause bias regardless of the estimators used.

Human Study

The clustering results at one slice level were shown in Fig. 5A. For 5 clusters, cluster 1 to cluster 5 correspond approximately to the regions of scalp, white matter, mixture of white matter and gray matter, gray matter, and sinus, respectively. If 4 clusters were chosen, cluster 3 (mixture of white matter and gray matter) and cluster 4 (gray matter) were merged as one cluster. If 3 clusters were selected, cluster 1 (scalp) and cluster 2 (white matter) further merged together as one cluster. The five components in the parameter space estimated from the 5 clusters were shown in Table 1.

Figure 5B was the corresponding initial estimates and constraints of K_1, k_2, k_3, and V_p. It showed that the linear component representation method was quite robust to the number of components. This may be due to the following reasons: (1) hierarchical cluster algorithm was used in clustering dynamic image data, (2) CRM is a liner regression model, and (3) due to spatial smoothing on the images generated by CRM, the initial estimates are less sensitive to the kinetic differences among clusters.

TABLE 1

Components Estimated From 5 Clusters

	Cluster 1	Cluster 2	Cluster 3	Cluster 4	Cluster 5
K_1	0.032	0.030	0.087	0.103	0.030
k_2	0.151	0.047	0.321	0.216	0.065
k_3	0.036	0.036	0.146	0.168	0.032
V_p	0.031	0.048	0.027	0.056	0.332

The parametric images of K_1, k_2, k_3, V_p, and K_i generated by WNLS and NLRRSC were shown in Fig. 6. The same input data set and initial estimates based on 4 clusters (see Fig. 5B) were used for both the WNLS and NLRRSC methods. Consistent with the computer simulation results, the image quality of the parametric images generated by NLRRSC was significantly better than that of WNLS. As shown in Fig. 7, the ROI values calculated for K_1, k_3, V_p directly from the parametric images generated by NLRRSC (x axis) had a higher linear correlation ($R^2 > 0.95$) with the values estimated from ROI kinetics by WNLS (y axis) compared to that for k_2 ($R^2 > 0.87$). For LCMRGlc, the highest linear correlation was obtained as: Y(ROI method) = 0.931X(NLRRSC image) +0.521 with $R^2 = 0.98$. Therefore, parametric images generated by NLRRSC gave values of the parameters as reliable as to those by the "ROI method."

The pixel-wise comparison between LCMRGlc calculated by NLRRSC and Patlak plot methods is shown in Fig. 8. The correlation of all pixel values was high $R^2 = 0.99$ (Fig. 8B) and could be expressed by:

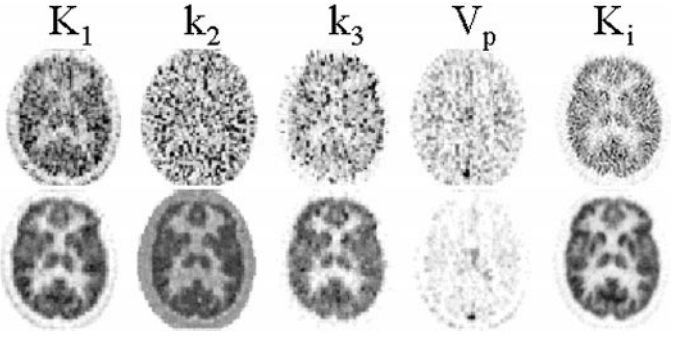

FIG. 6. The parametric images were generated by WNLS (top row) and NLRRSC (bottom row). The K_i ($K_1\ k_3/(k_2 + k_3)$) was calculated after pixel-wise model fitting. The same initial estimates obtained by component representation model analysis with four clusters (see Fig. 5B) were used for both WNLS and NLRRSC parametric imaging algorithms.

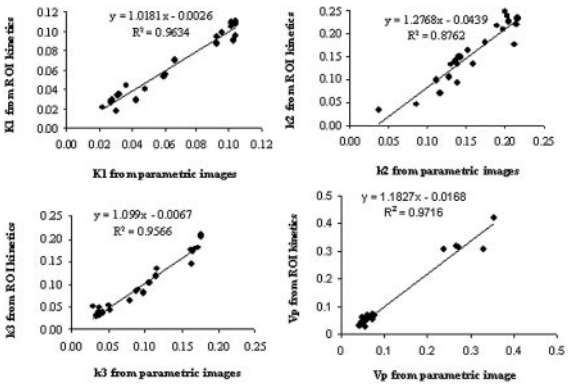

FIG. 7. A highly correlated linear relationship was observed between estimates from ROI kinetics and estimates from ROI means of parametric images generated by NLRRSC. 21 ROIs with each including at least 20 pixels were defined on the parametric images.

$$\text{NLRRSC (LCMRGlc)} = 1.05\,\text{Patlak(LCMRGlc)} + 0.075.$$

The LCMRGlc estimated by NLRRSC (with k_4 fixed at 0.004/min) was significantly higher (~5%) than that estimated by the Patlak plot method (paired T test, $P < 0.001$). This is consistent with previously reported FDG human studies in which the underestimation of LCMRGlc was attributed to the exclusion of dephosphorylation of FDG in the model (equivalent to the assumption for using Patlak) (Phelps *et al.*, 1979; Lammertsma *et al.*, 1987). These results suggest that NLRRSC provides a reliable estimate of LCMRGlc with a comparable or better image quality compared to Patlak analysis. However, it has a much larger computational burden. Thus, if only LCMRGlc is desired, Patlak analysis is still a more practical method to use.

Inclusion of the penalty term in the cost function resulted in improved convergence of the modeling. NLRRSC usually converged within 6 iterations for both the computer simulation and human study whereas, using the same initial estimates and convergence criteria, WNLS usually required more than 20 iterations. To generate a parametric image, it takes about 15 min for NLRRSC on an Ultra 5 SPARC workstation.

DISCUSSIONS

This study demonstrates that NLRRSC is a promising algorithm for the generation of parametric images of model microparameters derived from FDG dynamic studies. For NLRRSC, the variance of the estimates was reduced by ridge regression while the bias of estimates was limited by the constraints. The initial cluster analysis combined with the linear components representation model provides good initial estimates and constraint parameters that are helpful for (1) avoiding trapped in local minimum, and (2) limiting the bias due to ridge regression. The component representation model proved to be an efficiency method to obtain more accurate constraint and initial estimates for further analysis even though it is questionable that only a few of components exist in nature (Ashburner *et al.*, 1996). We chose hierarchical cluster analysis with average linkage method, although different techniques of cluster analysis for improving the signal-to-noise ratio of estimates have been used successfully by others (O'Sullivan, 1994; Kimura *et al.*, 1999; Feng *et al.*, 2001). In fact, some other cluster algorithm, such as hierarchical cluster analysis with ward linkage method, was also tried for the same data set in this study. It was found that Ward's method tends to join

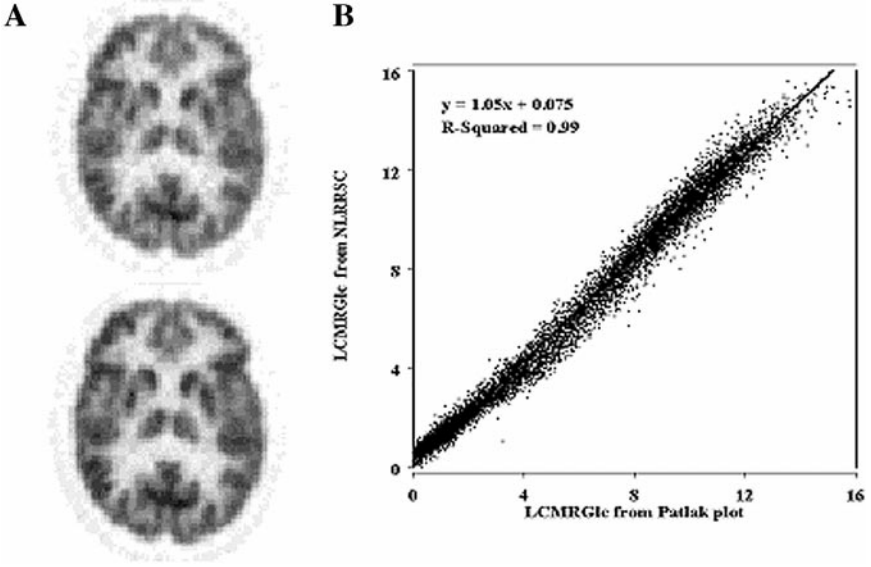

FIG. 8. Pixel-wise comparison of a parametric image of LCMRGlc estimated by Patlak plot and NLRRSC.

clusters with small numbers of observation and is strongly biased toward producing clusters with roughly the same number of observations. For example, sinus cluster is merged with other clusters by the ward linkage method. This finding is quite consistent with one comparison study reported before (Milligam, 1980).

Based on the theory of hierarchical cluster analysis with average linkage, the distance between two clusters depends on the magnitude as well as the shape of the curve of the two clusters—not just on the shape of the curve as in factor analysis. To ensure the expression in terms of the components to be unique for each pixel in the kinetic space and in the parameter space, it is necessary to choose the components with different curve shapes, i.e., no two components is parallel in kinetic space. It is obvious that the distance between components becomes smaller as the selected number of components (clusters) is increased. Since a major objective of CRM analysis in NLRRSC is to provide good initial estimates, it is not necessary to obtain exact representation of the pixel kinetics in terms of many cluster components. Also, to get a near exact representation is very time consuming as demonstrated by the cross validation procedure used by O'Sullivan (1994). The constraints on the weightings of the components (π_i) ensures that the initial estimate is a convex linear combination of the components, and will thus be less sensitive to the noise level of the pixel kinetics. In addition, the use of the spatially smoothed CRM solution as the initial estimate further reduces its sensitivity to the number of components (clusters) used. Figure 5 shows that the initial estimates or spatial constraints (both are the same) were in fact quite robust to the selected number of clusters. In general, 4 or 5 clusters were found to be appropriate for FDG study in normal subjects. Based on results shown in Fig. 5, an alternative way to extract components may be the conventional ROI approach, i.e., to obtain TACs of clusters by drawing the ROIs of gray, white, sinuous, scalp, and other possible regions if necessary, directly on PET or MRI images.

It is difficult to directly compare NLRRSC with conventional methods using smoothing techniques that apply linear spatial filters to the dynamic or parametric images. With NLRRSC, spatial constraint is incorporated into the parametric images via ridge regression. Ridge regression is less stringent in that the constraint in the parameter space is automatically adjusted by the noise level of the tracer kinetics. As a result, the "smoothing" of parametric images by NLRRSC is minimal but nonuniform.

In the computer simulation, we also tried two other filters (3×3, 7×7 windows, equal weighting for all pixels of filter). The results showed that the NLRRSC estimates using the three different filters are comparable in terms of RMSE% and parametric image quality. The filter (equal weighting over all pixels within given window) selected in the current study and our previous study was originated from the criterion of local variation in parametric image. In fact, any filter could be used in NLRRSC, and selection is always dependent on the noise level of the dynamic images.

In the human studies including normal control and trauma patients, we also tried k_4 values fixed in the range of 0 to 0.01/min, it seems that k_4 values between 0.004 and 0.006/min give acceptable results in terms of image quality and accuracy of the estimates.

The NLRRSC method used in this study has the same penalty weighting for all model parameters, and the same spatial filter was used for all mico-parametric images and ridge parameter image. The method can be easily extended to general NLRRSC with different penalty coefficients or different spatial filters for different microparameters. For general NLRRSC, the corresponding general linear ridge regression with spatial constraint (Zhou *et al.*, 2001a) can be used to determine the ridge parameters. Based on trade-off considerations between improvement in parametric image quality and computational burden, simple NLRRSC is likely to be a good compromise for dynamic studies that can be represented by a simple configuration tracer kinetic model (Zhou *et al.*, 2001a).

The NLRRSC algorithm utilized in this study was assessed exclusively using the FDG kinetic model. Theoretically, the algorithm could be applied directly to other dynamic PET studies as well as to dynamic single photon emission computed tomography (SPECT) studies. It is likely that as the tracer kinetic models become more complex or the number of parameters increase, the accuracy of the estimates may be improved more by NLRRSC when compared with conventional nonlinear regression algorithms.

In summary, the parametric images generated by the NLRRSC algorithm are superior to those created by conventional nonlinear regression methods. In the simulated FDG-PET studies, the RMSE% of NLRRSC estimates is 60–80% smaller compared to WNLS at a wide range of noise levels. For NLRRSC, since the mean square error was dominated by the variance term, the effect of bias on the reliability of the NLRRSC estimates was negligible. Results from a human FDG-PET study showed that NLRRSC gave parameter estimates that were as reliable as those obtained by the conventional ROI approach and by Patlak method.

ACKNOWLEDGMENTS

This work was partially supported by NIH Grant NINDS-30308 and DOE Contract DE-FC0387-ER60615.

REFERENCES

Anderberg, M. R. 1973. *Cluster Analysis for Applications.* Academic Press, New York.

Ashburner, J., Haslam, J., Taylor, C., *et al.* 1996. A cluster analysis approach for the characterization of dynamic PET data. In *Quantification of Brain Function Using PET* (Myers, R., Cunningham, V., Bailey, D., and Jones, T., Eds.), pp. 301–306. Academic Press, San Diego.

Bergsneider, M., Hovda, D. A., Shalmon, E., *et al.* 1997. Cerebral hyperglycolysis following severe human traumatic brain injury: A positron emission tomography study. *J. Neurosurg.* **86:** 241–251.

Blomqvist, G. 1984. On the construction of functional maps in positron emission tomography, *J. Cereb. Blood Flow Metab.* **4:** 629–623.

Blomqvist, G., Pauli, S., Farde, L., *et al.* 1990. Maps of receptor binding parameters in the human brain—A kinetic analysis of PET measurements. *Eur. J. Nucl. Med.* **16:** 257–265.

Blomqvist, G., Lammertsma, A. A., Mazoyer, B., Wienhard, K., 1995. Effects of tissue heterogeneity on quantification in positron emission tomography. *Eur. J. Nucl. Med.* **22:** 652–663.

Carson, R. E., Huang, S.-C., Green, M. V. 1986. Weighted integration method for local cerebral blood flow measurements with positron emission tomography. *J. Cereb. Blood Flow Metab.* **16:** 245–258.

Chen, K., Lawson, M., Reiman, E., *et al.* 1998. Generalized linear least squares method for fast generation of myocardial blood flow parametric images with N-13 Ammonia PET. *IEEE Trans. Med. Imag.* **17:** 236–243.

Choi, Y., Hawkins, R. A., Huang, S. C., *et al.* 1991. Parametric images of myocardial metabolic rate of glucose generated from dynamic cardiac PET and 2-[F-18]fluoro-2-deoxy-D-glucose studies. *J. Nucl. Med.* **32:** 733–738.

Cochran, W. G. 1977. *Sampling Techniques,* 3rd ed. Wiley, New York.

Cunningham, V. J., and Jones, T. 1993. Spectral analysis of dynamic PET studies. *J. Cereb. Blood Flow Metab.* **13:** 13–23.

Feng, D., Huang, S.-C., Wang, Z., *et al.* 1996. An unbiased parametric imaging algorithm for nonuniformly sampled biomedical system parameter estimation. *IEEE Trans. Med. Imag.* **15:** 512–518.

Feng, D., Cai, W., and Fulton, R. 2001. A reliable unbiased parametric imaging algorithm for noisy clinical brain PET data. In *Physiological Imaging of the Brain with PET* (Gjedde, A., Hansen, S. B., Knudsen, G. M., Paulson, O., Eds.), pp. 147–151. Academic Press, San Diego.

Frey, K. A., Holthoff, V. A., Koeppe, R. A., *et al.* 1991. Parametric *in vivo* imaging of benzodiazepine receptor distribution in human brain. *Ann. Neurol.* **30:** 663–672.

Gunn, R. N., Lammertsma, A. A., Hume, S. P., *et al.* 1997. Parametric imaging of ligand-receptor binding in PET using a simplified reference region model. *NeuroImage* **6:** 279–287.

Hartley, H. O. 1961. The modified Gauss-Newton method for the fitting of non-linear regression function by least squares. *Technometric* **3:** 269–280.

Hawkins, R. A., Phelps, M. E., and Huang, S.-C. 1986. Effects of temporal sampling, glucose metabolic rates, and disruptions of the blood–brain barrier on the FDG model with and without a vascular compartment: studies in human brain tumors with PET. *J. Cereb. Blood Flow Metab* **6:** 170–183.

Heiss, W. D., Pawlik, G., Herholz, K., *et al.* 1984. Regional kinetic constants and cerebral metabolic rate for glucose in normal human volunteers determined by dynamic positron emission tomography of [^{18}F]2-Fluoro-2-Deoxy-D-Glucose. *J. Cereb. Blood Flow Metab* **4:** 212–223.

Herholz, K. 1987. Nonstational spatial filtering and accelerated curve fitting for parametric imaging with dynamic PET. *Eur. J. Nucl. Med.* **14:** 477–484.

Herholz, K., and Patlak, C. S. 1987. The influence of tissue heterogeneity on results of fitting nonlinear model equations to regional tracer uptake curves: With an application to compartment models used in positron emission tomography. *J. Cereb. Blood Flow Metab.* **7:** 214–229.

Herscovitch, P., and Raichle, M. E. 1983. Effect of tissue heterogeneity on the measurement of cerebral blood flow with the equilibrium $C^{15}O_2$ inhalation technique. *J. Cereb. Blood Flow Metab.* **3:** 407–415.

Hoerl, A. E., and Kennard, R. W. 1970. Ridge regression: Biased estimation for nonorthogonal problems. *Technometrics* **12:** 55–67.

Hoerl, A. E., and Kennard, R. W., 1970. Ridge regression: Applications to nonorthogonal problems. *Technometrics* **12:** 69–82.

Hoffman, E. J., Ricci, A. R., St. Lmam, V. D., Phelps, M. E. 1983. ECAT III—Basic design considerations. *IEEE Trans. Nucl. Sci.* **30:** 729–733.

Huang, S.-C., Phelps, M. E., Hoffman, E. J., *et al.* (1980) Noninvasive determination of local cerebral metabolic rate of glucose in man. *Am. J. Physiol.* **238:** E69–E82.

Huang, S.-C., Phelps, M. E., Hoffman, E. J., and Kuhl, D. E. 1981. Error sensitivity of Fluorodeoxyglucose method for measurement of cerebral metabolic rate of glucose. *J. Cereb. Blood Flow Metab* **1:** 391–401.

Huang, S.-C., Zhou, Y. 1998. Spatially-coordinated regression for image-wise model fitting to dynamic PET data for generating parametric images. *IEEE Trans. Nucl. Sci.* **45:** 1194–1199.

Jovkar, S., Evans, A. C., Diksic, M., *et al.* 1989. Minimization of parameter estimation errors in dynamic PET: Choice of scanning schedules. *Phys. Med. Biol.* **34:** 895–908.

Kimura, Y., Hsu, H., Toyama, H., *et al.* 1999. Improved signal-to-noise ratio in parametric images by cluster analysis. *NeuroImage* **9:** 554–561.

Koeppe, R. A., Frey, K. A., Mulholland, G. K., *et al.* 1991. Compartmental analysis of [11C]flumazentil kinetics for the estimation of ligand transport rate and receptor distribution using positron emission tomography. *J. Cereb. Blood Flow Metab.* **11:** 735–744.

Lammertsma, A. A., Brooks, D. J., Frackowiak, R. S. J., *et al.* 1987. Measurement of glucose utilization with [^{18}F]2-Fluoro-2-Deoxy-D-Glucose: A comparison of different analytical methods. *J. Cereb. Blood Flow Metab.* **7:** 161–172.

Logan, J., Fowler, J. S., Volkow, N. D., *et al.* 1990. Graphical analysis of reversible radioligand binding from time-activity measurements applied to [*N*-11C-methuyl]-(−)-cocaine PET studies in human subjects. *J. Cereb. Blood Flow Metab.* **10:** 740–747.

Logan, J., Fowler, J. S., Volkow, N. D., *et al.* 1996. Distribution volume ratios without blood sampling from graphic analysis of PET data. *J. Cereb. Blood Flow Metab.* **16:** 834–840.

Marquardt, D. W. 1963. An algorithm for least-squares estimations of nonlinear parameters. *J. Soc. Ind. Appl Math.* **11:** 431–441.

Milligan, G. M. 1980. An examination of the effects of six types of error perturbation on fifteen clustering algorithms. *Psychometrika* **45:** 325–342

O'Sullivan, F. 1994. Metabolic images from dynamic positron emission tomography studies. *Stat. Methods Med. Res.* **3:** 87–101.

O'Sullivan, F. and Saha, A. 1999. Use of ridge regression for improved estimation of kinetic constraint from PET data. *IEEE Trans. Med. Imag.* **2:** 115–125.

Patlak, C. S., Blasber, R. G., and Fenstermacher, J. D. 1983. Graphical evaluation of blood-to-brain transfer constants from multiple-time uptake data. *J. Cereb. Blood Flow Metab.* **3:** 1–7.

Patlak, C. S., Blasber, R. G. 1985. Graphical evaluation of blood-to-brain transfer constants from multiple-time uptake data: Generalizations. *J. Cereb. Blood Flow Metab.* **5:** 584–590.

Phelps, M. E., Huang, S.-C., Hoffman, E. J., *et al.* 1979. Tomographic measurement of local cerebral glucose metabolic rate in human with (F-18) 2-fluoro-2-deoxy-D-glucose: Validation of method. *Ann. Neural.* **6:** 371–388.

Wu, H. M., Huang, S.-C., Choi, Y. *et. al.* 1995. A modeling method to improve quantitation of fluorodeoxyglucose uptake in heterogeneous tumor tissue. *J. Nucl. Med.* **36:** 297–306.

Zhou, Y., Huang, S.-C., Cloughesy, T., *et al.* 1997. A modeling-based factor extraction method for determing spatial heterogeneity of Ga-68 EDTA kinetics in brain tumors. *IEEE Trans. Nucl. Sci.* **44:** 2522–2527.

Zhou, Y., Huang, S.-C., and Bergsneider, M. 2001a. Linear ridge regression with spatial constraint for generation parametric images in dynamic positron emission tomography studies. *IEEE Trans. Nucl. Sci.* **48:** 125–130.

Zhou, Y., Huang, S. C., and Bergsneider, M. 2001b. Modelfitting with spatial constraint for parametric imaging in dynamic PET studies. In *Physiological Imaging of the Brain with PET* (Gjedde, A., Hansen, S. B., Knudsen, G. M., and Paulson, O., Eds.), pp. 159–163. Academic Press, San Diego.

Zhou, Y., Endres, C. J., Dogan, A. S., Brasic, J. R., Huang, S.-C., and Wong, D. F., 2001c. A new linear parametric imaging algorithm derived from simplified reference tissue model for ligand-receptor dynamic PET studies. In *Brain Imaging Using PET* (Senda, M., Kimura, Y., and Herscovitch, P., Eds.), in press. San Diego, Academic Press.